
Single Image Super-Resolution with Uncertainty Estimation for Lunar Satellite Images

Anonymous Author(s)

Affiliation

Address

email

Abstract

1 Recently, there has been a renewed interest in returning to the Moon, with many
2 planned missions targeting the south pole. This region is of high scientific and
3 commercial interest, mostly due to the presence of water-ice and other volatiles
4 which could enable our sustainable presence on the Moon and beyond. In order
5 to plan safe and effective crewed and robotic missions, access to high-resolution
6 (<0.5 m) surface imagery is critical. However, the overwhelming majority (99.7%)
7 of existing images over the south pole have spatial resolutions >1 m. In order to
8 obtain better images, the only currently available way is to launch a new satellite
9 mission to the Moon with better equipment to gather more precise data. In this work
10 we develop an alternative that can be used directly on previously gathered data and
11 therefore saving a lot of resources. It consist of a single image super-resolution (SR)
12 approach based on generative adversarial networks that is able to super-resolve
13 existing images from 1 m to 0.5 m resolution, unlocking a large catalogue of images
14 ($\sim 50,000$) for a more accurate mission planning in the region of interest for the
15 upcoming missions. We show that our enhanced images reveal previously unseen
16 hazards such as small craters and boulders, allowing safer traverse planning. Our
17 approach also includes uncertainty estimation, which allows mission planners to
18 understand the reliability of the super-resolved images.

19 1 Introduction

20 The Moon has been receiving increasing interest in recent years. Many upcoming missions have been
21 planned, for example in the frame of NASA’s Artemis program which aims to put humans back on
22 the Moon within this decade (Smith et al., 2020). A major goal is to achieve a permanent presence on
23 the Moon, and for many of these missions the south pole is the main target. This region is of high
24 scientific and commercial interest because it is expected to host water-ice and other resources which
25 could enable our sustainable presence.

26 High-resolution (HR) satellite imagery is essential for planning such missions. For example, when
27 planning human and rover traverses, mission planners need imagery with a resolution of $\sim 0.5\text{m/px}$ or
28 better to detect relevant features at the rover-/astronaut-scale, such as craters and boulders (Robinson
29 et al., 2010). This allows small hazards to be identified in advance, ensuring safe and efficient traverses.
30 Over the past 12 years NASA’s Lunar Reconnaissance Orbiter (LRO) mission has been capturing
31 state-of-the-art images of the lunar surface using its Narrow Angle Camera (NAC) (Robinson et al.,
32 2010), and their spatial resolutions typically vary in the range 0.5-2 m. However, at the south pole
33 the overwhelming majority of these images have resolutions $>1\text{m}$. This is due to the inherent low
34 lighting conditions. Over the south pole, most images (99.7%) are captured using what is known as
35 as “summed mode” operation of the NAC, which sums two adjacent pixels to improve SNR at the

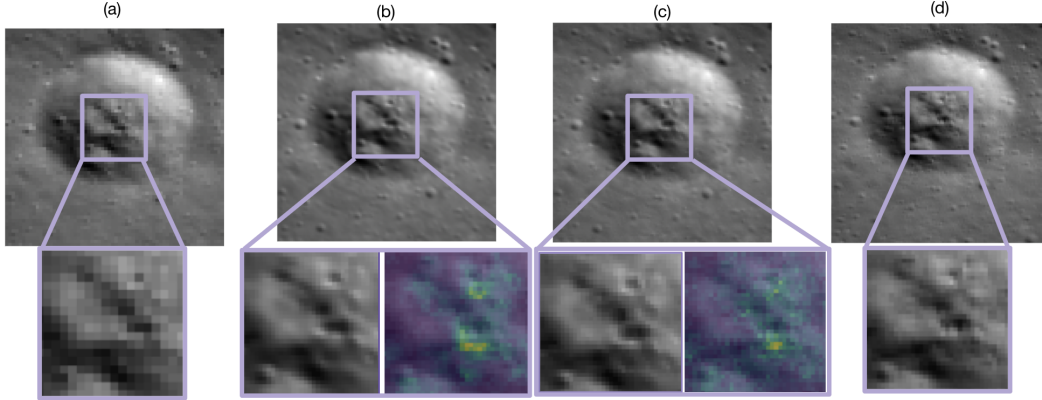


Figure 1: Using ANUBIS to super-resolve real LRO NAC imagery (Lat: -64.51 , Long: 299.6). (a) A real 1 m/px summed mode image, (b) after LSRRes (our work), (c) after LSRGAN (our work), (d) a coinciding real 0.5 m/px regular mode image (ground truth). The uncertainty map displayed next to the enhanced image shows our confidence in the super-resolved image (yellow: high uncertainty, purple: low uncertainty).

36 expense of reducing resolution by a factor of 2 (Humm et al., 2015). Unfortunately, this limits their
 37 usefulness for mission planning.

38 In this work we introduce ANUBIS (Adversarial Network for Uncertainty-Based Image Super-
 39 resolution). ANUBIS uses a deep ensemble of GANs to super-resolve these images, increasing
 40 their resolution by a factor of 2 (from 1 m to 0.5 m), providing enhanced data products for mission
 41 planners. We show that these images enable safer traverse planning, and by using an ensemble we are
 42 also able to output uncertainty estimates, which is essential for their safety-critical application.

43 2 Methodology

44 The main goal of this work is to learn to super-resolve existing summed-mode NAC images over the
 45 south pole from $\sim 1\text{m/px}$ to $\sim 0.5\text{m/px}$. We note that a small number of “regular mode” images over
 46 the south pole are taken without the summing operation which have $\sim 0.5\text{m/px}$ resolution. These
 47 images are not common ($\sim 0.0028\%$), but there are enough examples with high SNR to construct a
 48 labelled training dataset. An example regular mode image is shown in Figure 1 (d).

49 Specifically, we generate a training, validation, and testing data starting from 121 ($52,224 \times 5,064\text{ px}$)
 50 regular mode NAC images of the south pole. The selected images have a resolution of 0.5 ± 0.05
 51 m/px and similar illumination conditions to the summed mode polar images. We divide the images
 52 into 128×128 patches, resulting in 220,000 HR patches. To approximate the NAC summed mode,
 53 we apply a local 2×2 mean and round to the next integer value to obtain their low-resolution
 54 (LR) $\sim 1\text{m/px}$ counterparts. This operation represents a best effort approach to approximate the real
 55 summing performed on the spacecraft. We split this dataset into a training, validation and test dataset
 56 using a 80:10:10 split.

57 Two separate single image SR approaches are designed. The first uses a residual network (LSRRes)
 58 which takes a LR image and outputs a HR image, trained with an L2 loss function. The second builds
 59 on the first, training LSRRes with an additional adversarial loss (LSRGAN), and is shown in Figure 2.
 60 The goal of this approach is to ensure the output image is as realistic as possible via the interaction of
 61 the generator (LSRRes) and discriminator network.

62 A major concern when using single image SR is the potential for generating artifacts (or “hallucina-
 63 tions”), which are generally related to the ill-posedness of the inverse problem. This is of key concern
 64 in our application, as mission planners will use our images in safety-critical applications. Thus to
 65 increase the reliability of our images we also explore uncertainty estimation. Specifically, we train
 66 an ensemble of 24 LSRGANs with different weight initialisations, allowing us to output multiple
 67 realisations of the same super-resolved image. Each realisation differs slightly due to ill-posedness of
 68 the problem. The pixel-wise standard deviation of these images is used to generate an uncertainty

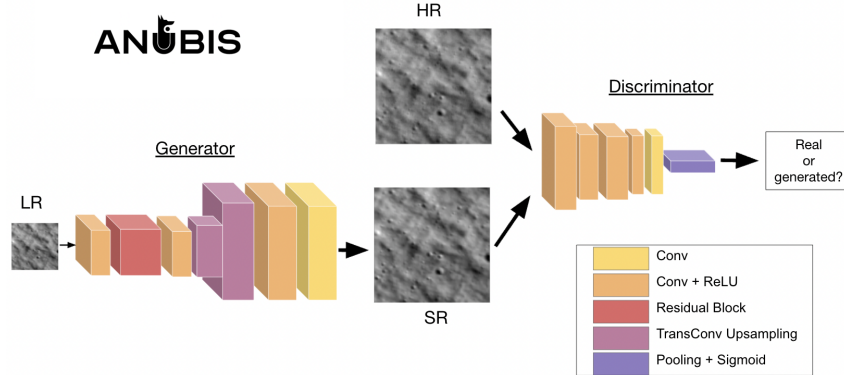


Figure 2: The ANUBIS LSRGAN architecture, consisting of a residual generator and a fully-convolutional discriminator. Colors indicate different block types.

| Method | MAE↓ | PSNR↑ | SSIM↑ |
|---------------|---------------|--------------|--------------|
| LR | 0.0042 | 44.81 | 0.9745 |
| Bilinear | 0.0037 | 45.89 | 0.979 |
| Bicubic | 0.0032 | 47.26 | 0.984 |
| LSRGAN (ours) | 0.0034 | 47.23 | 0.983 |
| LSRRes (ours) | 0.0027 | 49.13 | 0.989 |

Table 1: Performance of SR methods on our test set. Best scores in bold. The LSRRes/LSRGAN metrics are computed using only a single randomly selected ensemble member.

69 map, which provides an estimate of the reliability of our SR process. The same uncertainty workflow
 70 is carried out for the LSRRes-only approach too. All training details are described in Appendix A.

71 3 Results and discussion

72 An example real 1 m/px summed mode image over the south pole is shown in Figure 1 (a), and the
 73 result after applying LSRRes and LSRGAN (using a single randomly selected ensemble member) is
 74 shown in (b) and (c). A real 0.5 m/px regular mode image is also available over this region, and is
 75 shown in (d). We find that both LSRRes and LSRGAN are able to significantly enhance the resolution
 76 of the LR image, revealing small craters and other surface features which are present in the HR image
 77 and difficult to see in the LR image. When evaluating more images, we find that LSRGAN tends
 78 to output images with higher perceptual quality than LSRRes. Specifically, LSRGAN adds more
 79 small scale features such as craters and boulders to the image compared to LSRRes, resulting in a
 80 frequency spectrum which is more comparable to ground truth HR images.

81 We evaluate the quantitative performance of our methods on our test set of images, shown in Table 1.
 82 As metrics, we consider the mean absolute error (MAE), peak signal to noise ratio (PSNR), and
 83 structural similarity index measurement (SSIM). We also compare our methods to two baseline
 84 approaches (bilinear and bicubic interpolation). Under these metrics, we find that LSRRes gives
 85 the highest performance. However, given the improved perceptual quality of the LSRGAN images
 86 observed above, these metrics may not be the best suited for this task.

87 We also show the uncertainty maps generated by our ensembles of LSRRes/LSRGANs for the super-
 88 resolved images in Figure 1. These maps are most uncertain around crater rims, which is believable
 89 as they represent high-frequency features in the image which are likely difficult to reconstruct.

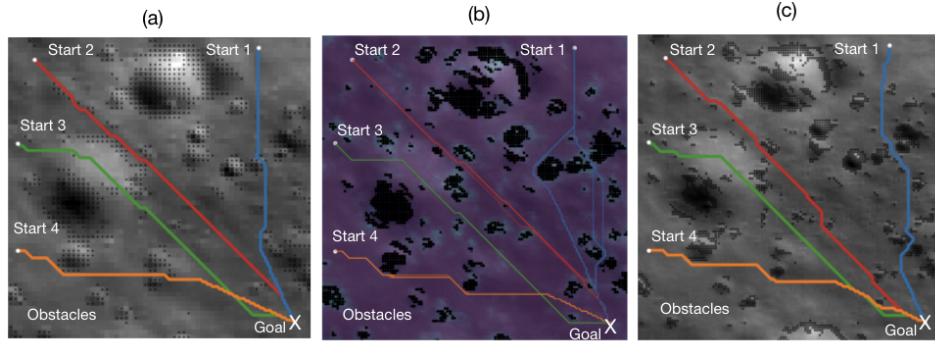


Figure 3: Validating ANUBIS with traverse planning. (a) Low-resolution (input), (b) Super-resolution + Uncertainty map (our work), (c) High-resolution (Ground truth).

90 4 Validation with traverse planning

91 Finally, we show the value of our super-resolved images on a downstream task, here: traverse
 92 planning. We set up a hypothetical problem, where a rover must plan a safe traverse from its starting
 93 position to a goal, given an image and the locations shown in Figure 3. Given an image, we detect
 94 obstacles based on the image gradients and then use an A* path planning algorithm to plan a safe
 95 traverse around them. During path planning using our super-resolved images, we also add obstacles
 96 derived from our uncertainty map (using the same obstacle detection process, i.e., high uncertainty
 97 pixels are considered as obstacles). Figure 3 shows the resulting traverses when using a LR summed
 98 mode image, its super-resolved version using LSRGAN, and a ground truth regular mode HR image.
 99 We find that for this location the LSRGAN paths more closely match the HR image paths than the
 100 LR image paths, i.e. allowing for a safer and more efficient traverse.

101 5 Limitations and future work

102 There are multiple limitations and future directions of our work. Firstly, we restricted ourselves to
 103 only learning a mapping from 1 m/px to 0.5 m/px, whereas in reality NAC images of the south pole
 104 span a range of resolutions >1 m/px. In future work, we aim to develop a workflow which is able to
 105 learn a mapping from any input resolution to any output resolution, within reason, allowing more
 106 NAC images to be super-resolved. Secondly, there are many other uncertainty estimation techniques
 107 which could be tested. For example, GANs with random input vectors (Abid et al., 2021), normalising
 108 flows (Lugmayr et al., 2020), dropout or other Bayesian inference approaches could be more effective.
 109 Finally, we assume that our downsampling operator can be approximated by a simple summation and
 110 rounding. However, in reality NAC images are subject to a lossy compression before downlink to
 111 Earth (Robinson et al., 2010), and therefore this degradation process is not modelled; we intend to
 112 include this in future work.

113 6 Conclusions and broader impact

114 We have investigated methods for super-resolving lunar imagery over the south pole by a factor
 115 of 2 (from 1 m/px to 0.5 m/px) and shown that they can improve image quality and help achieve
 116 downstream tasks such as traverse planning. Furthermore we provided uncertainty estimates for
 117 each super-resolved image, which is essential for safety-critical applications. Our approach provides
 118 higher resolution images over the south pole of the Moon, where they are not currently available,
 119 allowing mission planners to plan safer and more effective missions.

120 This work could have a positive impact on the planning and execution of future lunar exploration
 121 missions, specifically by reducing their risk and maximizing their efficacy. The uncertainty maps
 122 that are delivered along with the improved images greatly increase the reliability of ANUBIS for
 123 safety-critical applications. Upcoming robotic and crewed missions, such as NASA’s VIPER or other
 124 Artemis missions, are a few of many possible beneficiaries of our work.

125 **References**

126 Abid, M. A., Hedhli, I., and Gagné, C. (2021). A generative model for hallucinating diverse versions
127 of super resolution images. *arXiv preprint arXiv:2102.06624*.

128 Humm, D., Tschimmel, M., Brylow, S., Mahanti, P., Tran, T., Braden, S., Wiseman, S., Danton, J.,
129 Eliason, E., and Robinson, M. (2015). Flight calibration of the Iroc narrow angle camera. *Space*
130 *Science Reviews*, 200.

131 Lugmayr, A., Danelljan, M., Van Gool, L., and Timofte, R. (2020). SrfLOW: Learning the super-
132 resolution space with normalizing flow. In *European Conference on Computer Vision*, pages
133 715–732. Springer.

134 Robinson, M., Brylow, S., Tschimmel, M., Humm, D., Lawrence, S., Thomas, P., Denevi, B.,
135 Bowman-Cisneros, E., Zerr, J., Ravine, M., et al. (2010). Lunar reconnaissance orbiter camera
136 (Iroc) instrument overview. *Space science reviews*, 150(1-4):81–124.

137 Smith, M., Craig, D., Herrmann, N., Mahoney, E., Krezel, J., McIntyre, N., and Goodliff, K. (2020).
138 The artemis program: An overview of nasa’s activities to return humans to the moon. In *2020*
139 *IEEE Aerospace Conference*, pages 1–10. IEEE.

140 **A Training details**

141 Our LSRRes network uses a convolutional residual architecture with 6 layers, and ReLU activation
142 functions (Generator section in Fig. 2). The discriminator in our LSRGAN uses a convolutional
143 architecture with 6 layers, and ReLU activation functions. All approaches were trained using the
144 Adam optimizer, a learning rate of 0.0002 and a batch size of 256. The inputs and outputs of the
145 networks are normalised before training. Training takes approximately 3 hours on a single NVIDIA
146 Tesla A100 GPU.

147 To create the deep ensemble of GANs used to generate the SR image distribution, the same architecture
148 was trained 24 different times using random weight initialization.

149 **B NeurIPS 2021 Paper Checklist**

- 150 1. *Do the main claims made in the abstract and introduction accurately reflect the paper’s*
151 *contributions and scope?: Yes*
- 152 2. *Have you read the ethics review guidelines and ensured that your paper conforms to them?:*
153 *Yes*
- 154 3. *Did you discuss any potential negative societal impacts of your work?: Yes*
- 155 4. *Did you describe the limitations of your work?: Yes*
- 156 5. *Did you include the code, data, and instructions needed to reproduce the main experimental*
157 *results (either in the supplemental material or as a URL)?:* The data used during this work is
158 publicly available at <https://www.lroc.asu.edu/>. The code will be released in a future
159 journal publication.
- 160 6. *Did you specify all the training details (e.g., data splits, hyperparameters, how they were*
161 *chosen)?:* Yes
- 162 7. *Did you report error bars (e.g., with respect to the random seed after running experiments*
163 *multiple times)?:* Yes, with the uncertainty estimation.
- 164 8. *Did you include the amount of compute and the type of resources used (e.g., type of GPUs,*
165 *internal cluster, or cloud provider)?:* Yes